Coating Layers on Bed Particles during Biomass Fuel Combustion in Fluidized-Bed Boilers

Laura H. Nuutinen,[†] Minna S. Tiainen,[†] Mika E. Virtanen,[†] Sonja H. Enestam,[‡] and Risto S. Laitinen*[,†]

Department of Chemistry, P.O. Box 3000, 90014 University of Oulu, Finland, and Kvaerner Power Oy, P.O. Box 130, 01600 Vantaa, Finland

Received April 18, 2003. Revised Manuscript Received October 7, 2003

Adhesive coating layers on bed particles have been thought to be the cause of the agglomeration in fluidized-bed combustion. The formation of coating layers on particles of different bed materials (quartz, natural sand, and GR Granule) has been studied when the fluidized-bed combustion of various biomass fuels (bark, different types of wood fuel, peat, biosludge, chicken litter, REF, and forest residue) occurs. The bed samples have been collected during the laboratory-scale, pilot-scale, and full-scale boiler tests. The chemical composition of the coating layers were characterized by scanning electron microscopy, coupled with energy-dispersive spectroscopy (SEM-EDS), through the utilization of line scans, as well as point and domain analyses. X-ray maps were also recorded to characterize the coating layers. The coatings on the bed particles often consisted of several superimposed layers. The innermost layer mainly contained alkali silicates, whereas the outermost layer was rich in calcium or magnesium, depending on the composition of both the bed and the fuel. Coating layers that contain potassium or sodium may be adhesive and cause the formation of agglomerates, which would explain why quartz and natural sand bed materials are problematic when fuels with high alkali-metal content are combusted. The magnesium-containing coating layers on the GR Granule particles may protect the bed particles from agglomeration, and, consequently, this bed material can be used in the combustion of otherwise problematic fuels.

Introduction

The interest in fluidized-bed combustion has increased recently, because it has been found suitable for low-heat-capacity fuels. The availability and the environmental issues associated with biomass fuels and waste materials has made them an alternative source of energy and has increased their use in energy production during the past decade. Biomass fuels are considered CO_2-free, because they do not increase the net CO_2 emissions into the atmosphere. The fluidized-bed combustion of biomass and waste materials, however, is not always unproblematic. These problems, such as slagging, fouling, and agglomeration, are usually ash-related.

The agglomeration of bed material is one of the major problems in fluidized-bed combustion. In the worst case, it can lead to total defluidization of the bed and the nonscheduled shutdown of the entire power plant. The tendency toward agglomeration depends on the bed material, the fuel, the additives, and the boiler conditions.[1−4]

Although the mechanism of the bed agglomeration is not yet fully understood, several suggestions have been made.[5−9] Öhman and co-workers studied the bed agglomeration of biomass fuels extensively.[8,10−12] They expectedly found that the agglomeration process is

* Author to whom correspondence should be addressed. E-mail: Risto.Laitinen@oulu.fi.

[†] University of Oulu.

[‡] Kvaerner Power Oy.

(1) Lin, C. H.; Teng, J. T.; Chyang, C. S. Evaluation of the Combustion Efficiency and Emission of Pollutants by Coal Particles in a Vortexing Fluidized Bed. *Combust. Flame* **1997**, *110*, 163−172.

(2) Lin, W.; Dam-Johansen, K. Agglomeration in Fluidized Bed Combustion of Biomass—Mechanisms and Co-firing with Coal. In *15th International Conference on Fluidized Bed Combustion* (Savannah, GA, 1999); Reuther, R. B., Ed.; American Society of Mechanical Engineers (ASME): New York, 1999; p 12.

(3) Dawson, M. R.; Brown, R. C. Bed Material Cohesion and Loss Fluidization during Fluidized Bed Combustion of Midwestern Coal. *Fuel* **1992**, *71*, 585−592.

(4) Öhman, M.; Nordin, A. The Role of Kaolin in Prevention of Bed Agglomeration during Fluidized Bed Combustion of Biomass Fuels. *Energy Fuels* **2000**, *14*, 618−624.

(5) Anthony, E. J.; Iribarne, A. P.; Iribarne, J. V. A New Mechanism for FBC Agglomeration and Fouling When Firing 100% Petroleum Coke. In *Fluidized Bed Combustion*; American Society of Mechanical Engineers (ASME): New York, 1995; Vol. 1, pp 523−533.

(6) Rizeq, R. G.; Shadman, F. Alkali-Induced Agglomeration of Solid Particles in Coal Combustors and Gasifiers. *Chem. Eng. Commun.* **1989**, *81*, 83−96.

(7) Visser, H. J. M.; Hofmans, H.; Huijnen, H.; Kastelein, R.; Kiel, J. H. A.
Biomass Ash—Bed Material Interactions Leading to Agglomeration in Fluidised Bed Combustion and Gasification. In *Progress in Thermochemical Biomass Conversion*; Bridgwater, A. V., Ed.; Blackwell Science: Cornwall, U.K., 2001; Vol. 1, pp 272−286.

(8) Öhman, M.; Nordin, A.; Skrifvars, B.-J.; Backman, R.; Hupa, M. Bed Agglomeration Characteristics during Fluidized Bed Combustion of Biomass Fuels. *Energy Fuels* **2000**, *14*, 169−178.

(9) Ergudenler, A.; Ghaly, A. E. Agglomeration of Silica Sand in a Fluidized Bed Gasifier Operating on Wheat Straw. *Biomass Bioenergy* **1993**, *4*, 135−147.

(10) Öhman, M.; Nordin, A. A New Method for Quantification of Fluidized Bed Agglomeration Tendencies: A Sensitivity Analysis. *Energy Fuels* **1998**, *12*, 90−94.

(11) Öhman, M.; Nordin, A. Summary of Recent Results Obtained from Using the Controlled Fluidised Bed Agglomeration Method. In *Impact of Mineral Impurities in Solid Fuel Combustion*; Gupta, R. P., Wall, T. F., Baxter, L., Eds.; Kluwer: New York, 1999; pp 259−270.

(12) Öhman, M.; University of Umeå, Umeå, Sweden, 1999.

10.1021/ef0300850 CCC: $27.50
Published on Web 12/16/2003

Table 1. Experimental Setup

boiler test	fuel mixture	bed material	boiler	test duration	temp range, minimum−maximum (°C)
LS1	wood residue	quartz	laboratory-scale (BFB)		n.a.[a]
LS2	bark	quartz	laboratory-scale (BFB)		n.a.[a]
LS3	peat	quartz	laboratory-scale (BFB)		n.a.[a]
PS1	REF	natural sand	pilot-scale (3 kW, BFB)	3 h, 30 min	737−880
PS2	peat	natural sand	pilot-scale (3 kW, BFB)	3 h	715−877
PS3	biosludge	natural sand	pilot-scale (3 kW, BFB)	6 h, 20 min	697−886
PS4	chicken litter	natural sand	pilot-scale (3 kW, BFB)	1 h	804−889
PS5	plywood and wood	GR Granule	pilot-scale (3 kW, BFB)	5 h, 40 min	745−867
PS6	chicken litter	GR Granule	pilot-scale (3 kW, BFB)	25 min	792−972
FS1	bark, plywood, and biosludge	natural sand	full-scale (110 MW, BFB)		n.a.[a]
FS2	wood (Salix and chips)	natural sand	full-scale (45 MW, CFB)		870
FS3	wood (no Salix)	natural sand	full-scale (45 MW,CFB)		850
FS4	recycled wood	natural sand	full-scale (25 MW, CFB)		820
FS5	forest residue	natural sand	full-scale (30 MW, CFB)		850
FS6	REF and rubber	natural sand	full-scale (30 MW, CFB)		850
FS7	wood and industrial residue	GR granule	full-scale (7 MW, BFB)		n.a.[a]
FS8	wood and industrial residue	GR granule	full-scale (7 MW, BFB)		850
FS9	wood and peat	GR granule	full-scale (30 MW, CFB)		850
FS10	plywood waste and sawdust	GR granule	full-scale (6 MW, BFB)		829−910
FS11	plywood waste	GR granule	full-scale (5 MW, BFB)		834
FS12	plywood waste, dust, and bark	GR granule	full-scale (25 MW, BFB)		n.a.[a]
FS13	plywood waste and bark	GR granule	full-scale (15 MW, BFB)		n.a.[a]

[a] Not available.

dependent on the chemical characteristics and the melting behavior of the coatings, which were determined to be sensitive to the relative amounts of calcium and potassium in the fuel. As the potassium content increased, the coatings contained a larger fraction of the melt at the temperatures <900 °C. On the other hand, the coating with a high calcium content contained a significant amount of molten material only at temperatures well above 900 °C. The melt formation may cause the mutual adherence of the bed particles and may therefore be considered to be responsible for the agglomeration.

Visser et al.[7] suggested two different routes for agglomeration: "melt-induced" agglomeration and "coating-induced" agglomeration. In "melt-induced" agglomeration, the bed particles adhere together by a molten phase, the chemical composition of which resembles that of ash. This type of agglomeration can be attributed to be dependent on high local peak temperatures. "Coating-induced" agglomeration is considered to be more common. In that case, a coating layer is formed on the surface of bed particles. Under certain critical conditions (e.g., temperature and coating thickness), neck formation may occur between coatings of individual grains, which can initiate the agglomeration. After the first neck formation, partial defluidization of the bed leads to local regions of high temperatures. At these higher temperatures, the melt formation may occur and agglomeration can then proceed with both types of processes.

The present work was conducted to explore the formation of the coating layers on particles of different bed materials during the fluidized-bed combustion of various biomass fuels. The bed samples were collected during the laboratory-scale, pilot-scale, and full-scale boiler tests, and the chemical composition of the coating layers were characterized by scanning electron microscopy, coupled with energy-dispersive spectroscopy (SEM-EDS), through the utilization of line scans, as well as point and domain analyses. X-ray maps were also recorded, to characterize the coating layers. The compositional trends within the coating layers could be established and utilized to discuss the factors that affect the agglomeration propensity within the bed.

Experimental Details

Samples. The samples were collected from several boilers, ranging from laboratory-scale to full-scale boilers, using different bed materials (quartz, natural sand, and GR Granule). The bed materials, the fuel mixtures, the bed temperatures, and the scale of the boiler are described in Table 1. Testing for samples LS1−LS3 involved a laboratory-scale boiler, that for samples PS1−PS6 involved a pilot-scale boiler, and that for samples FS1−FS13 involved the normal operation of full-scale boilers. The combustion times were not reported for the laboratory-scale tests[8] and were not recorded during the full-scale tests. The duration of the pilot-scale tests ranged from 0.5 h to 6.5 h, and the samples were collected at the end of each test (see Table 1). The bed consumption was kept constant in these tests. The fuels used in the laboratory-scale, pilot-scale, and full-scale tests are from different origins and, therefore, are not directly comparable. The bed temperatures in different tests were relatively similar (see Table 1).

Elemental Analyses. The sample preparation for the inductively coupled plasma−optical emission spectroscopy (ICP−OES) determinations (for Na, Mg, Al, Si, P, K, Ca, Ti, and Fe) of fuels used in the pilot-scale tests were performed according to ASTM standard D 3682, by mixing the bed samples with $Li_2B_4O_7$. The determination of the sulfur content was done according to ASTM standard D 4208, using a Leco-S analyzer. The ashing of fuels from full-scale tests was done in 575 °C. The determinations of other elements were performed from fuel ash, using X-ray fluorescence (XRF).

SEM-EDS. Bed samples from all tests were characterized using a JEOL model JSM-6400 SEM microscope that was combined with a Link ISIS energy-dispersive X-ray analyzer. The acceleration voltage of 15 kV and a beam current of 12×10^{-8} A were used for the SEM-EDS analysis. The beam current during the recording of the X-ray maps was 67×10^{-8} A (for test samples FS10−FS14) or 57×10^{-8} A (for test samples FS1−FS9, PS1−PS6, and LS1−LS3). The sample distance was 15 mm. All SEM samples were mounted with epoxy resin (Struers Epofix, 15:2). Mounts were cross-sectioned by grinding with 250, 600, and 1200 mesh sandpaper. Finally, the samples

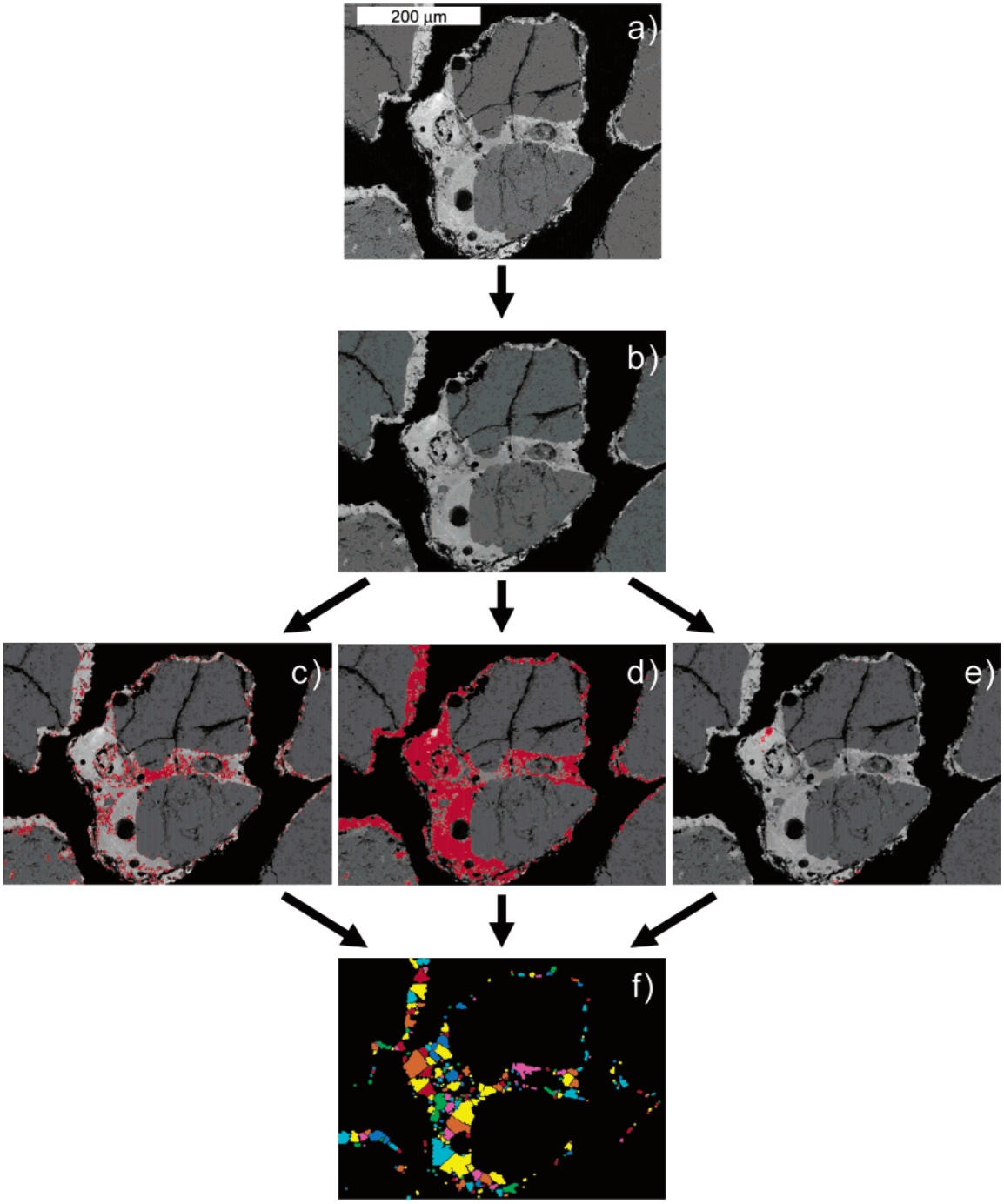

Figure 1. Depiction of the image processing procedure. Panel **a** shows a backscattered electron (BE) image of a bed agglomerate (160× magnification), whereas panel **b** shows the BE image after gray-scale operations. Panels **c**−**e** show three different gray-scale ranges activated (shown as red), and panel **f** shows the activated areas shown together after the arbitrary division of the large area in panels **c** and **d** into subdomains.

were coated with a thin carbon layer, to eliminate the electrostatic effects.

The SEM-EDS analysis was performed as described by Virtanen et al.[13] The backscattered electron (BE) image in SEM was collected using a resolution of 256 × 208 pixels. In BE images, the heavier elements appear brighter than the lighter elements (see panel **a** in Figure 1). The epoxy background in the samples appears black, and the bed material that contains relatively light elements are the darkest of the gray areas in the image. The coating layers and the adhesive material of agglomerates that generally contain heavy metals appear as brighter areas.

The original image was digitally smoothed to facilitate further treatment (see panel **b** in Figure 1). Because the coating layers and the adhesive material of the agglomerates appear brighter in the SEM image, they are considered separately by extracting two or three binary images, based on their level of grayness, from the smoothed BE image (see panels **c**−**e** in Figure 1). Because of possible variations in the elemental composition in the seemingly uniform gray areas, these regions were further arbitrarily divided into smaller domains (see panel **f** in Figure 1). The elemental composition of each domain has been determined individually. In this

(13) Virtanen, M. E.; Tiainen, M. S.; Laitinen, R. S. SEM-EDS and Image Analysis in the Characterisation of Coatings and Adhesive Material in the Quartz-Bed. In *5th European Conference on Industrial Furnaces and Boilers* (Porto, Portugal); INFUB: Rio Tinto, Portugal, 2000; pp 117−126.

Table 2. Bed Materials and Average Chemical Composition of Bed Particle Types

component	occurrence in bed[a]	Content (%) Na	Mg	Al	Si	K	Ca	Fe
		Quartz						
silicon dioxide	M				100			
		Natural Sand						
silicon dioxide	C				100			
potassium aluminosilicate	m			16	57	24		
sodium aluminosilicate	m	9		19	68			
sodium calcium aluminosilicate	t	6		24	56		14	
		GR Granule						
silicon dioxide	i, t				100			
potassium aluminosilicate	i, t			16	51	30		
sodium aluminosilicate	i, t	9		20	65			
sodium calcium aluminosilicate	i, t	6		24	55		13	
GR granule	M[b]							
magnesium iron silicate	t		50		40			10

[a] Legend for table is as follows: M, major (>80% of the bed material); C, common (occurrences of 30%−60% in bed material); m, minor (occurrences of 10%−30% in bed material); t, trace (<10% of the bed material); and i, impurities in bed material. [b] Proprietary information.

manner, the ZAF-corrected relative amounts of sodium, magnesium, aluminum, silicon, sulfur, phosphorus, potassium, calcium, titanium, and iron were determined for ca. 1000 domains from 5−10 fields within the sample. The image processing was performed with IMQuant software that was incorporated in the Link ISIS equipment.

The X-ray maps and the phase relationship images were created with the software in the Link ISIS equipment. The phase relationship images were produced from three elemental X-ray maps by coloring each map with one color (red, green, or blue) and integrating the colored maps into one image. The point analyses and line scans were made using the INCA program package that was incorporated in the Link software. More than 10 point analyses were made from each of the observed coating layers. However, if the coating layers were very thin (<10 μm), five point analyses were considered to be sufficient.

Quasi-ternary Diagrams. The SEM-EDS results from both the domain analyses and the point analyses were visualized using quasi-ternary diagrams that involved a locally designed software package.[13−15]

The quasi-ternary diagrams are a logical extension of the conventional ternary diagrams in which each corner has been defined in terms of a content of a single element. The content of this element is 100%, and it decreases toward the edge between the other two corners, being 0% at the opposite edge. At any point in the ternary diagram, the sum of the contents of the three elements is 100%.

In a quasi-ternary diagram, each corner can be defined in terms of several elements, with their combined contents being 100% at the corner. A general point in the quasi-ternary diagram contains compositional information about all elements defined in the three corners. For a point analysis to appear in the diagram, the sum of the contents of the chosen elements must exceed a minimum limit, usually 80%.[16] Let a corner be defined in terms of the sum of the contents of aluminum and silicon. The analytical results appear in this corner, if the combined aluminum and silicon contents are at least 80%. The diagram provides no information about the relative amounts of silicon and aluminum, and there can be up to 20% other elements that have not been defined in any of the three corners. As a general point, the sum of the contents of all elements defined in the three corners is 80%−100%. The column heights in the quasi-ternary diagrams represent the relative contents of the material with the elemental composition, as controlled by the definitions in the corners.

Results and Discussion

General. The bed materials considered in this work are described in Table 2. Each material is a heterogeneous mixture that contains several different particles. The chemical compositions of the particles in different bed materials were determined by SEM-EDS and are given in Table 2. The quartz bed used in the laboratory-scale tests contained 98% SiO_2.[8] The natural sand, in addition to SiO_2 particles, also contains sodium and potassium aluminosilicate and sodium calcium aluminosilicate particles. GR Granule does not contain SiO_2 particles, except as an impurity. Other minor components in this bed were magnesium iron silicates. (Note: The composition of GR Granule is proprietary information.)

The average compositions of the ash of different fuels used in this work are presented in Figures 2 and 3. Note that the full-scale tests involved different fuels from the pilot-scale tests. The ash compositions of the fuels considered in the laboratory-scale tests have been reported previously by Öhman et al.[8]

The compositional distributions in the bed material can be presented in quasi-ternary diagrams that are based on domain analyses, and they are exemplified by test samples PS3, FS1, PS5, and PS6 (see Figure 4). The testing of sample PS3 involves the combustion of biosludge and bark, and that of sample FS1 involves the combustion of plywood and biosludge. A natural sand bed is used in both cases. In test samples PS5 and PS6, wood and chicken litter, respectively, have been combusted in a GR Granule bed. The compositional distributions within the bed particles are expectedly dependent on the nature of the bed material and are insensitive to the use of different fuel types.

The major distribution maxima are due to the material in the actual bed particles. The BE images show,

(14) Virtanen, M. E.; Tiainen, M. S.; Pudas, M.; Laitinen, R. S. Visualization and Analysis of SEM-EDS Data of Quartz-Bed Agglomerates. In *Progress in Thermochemical Biomass Conversion*; Bridgwater, A. V., Ed.; Blackwell Science: Cornwall, U.K., 2001; Vol. 1, pp 671−677.

(15) Virtanen, M.; Tiainen, M.; Nuutinen, L.; Pudas, M.; Laitinen, R. A Tool for Visualization and Statistical Analysis of SEM-EDS Data. In *Effects of Coal Quality on Power Plant Performance: Ash Problems, Management and Solutions*; Mehta, A. K., Benson, S. A., Eds.; United Engineering Foundation: Park City, UT, 2001; pp 117−130.

(16) Helble, J. J.; Srinivasachar, S.; Boni, A. A. Factors Influencing the Transformation of Minerals During Pulverized Coal Combustion. *Prog. Energy Combust. Sci.* **1990**, *16*, 267−280.

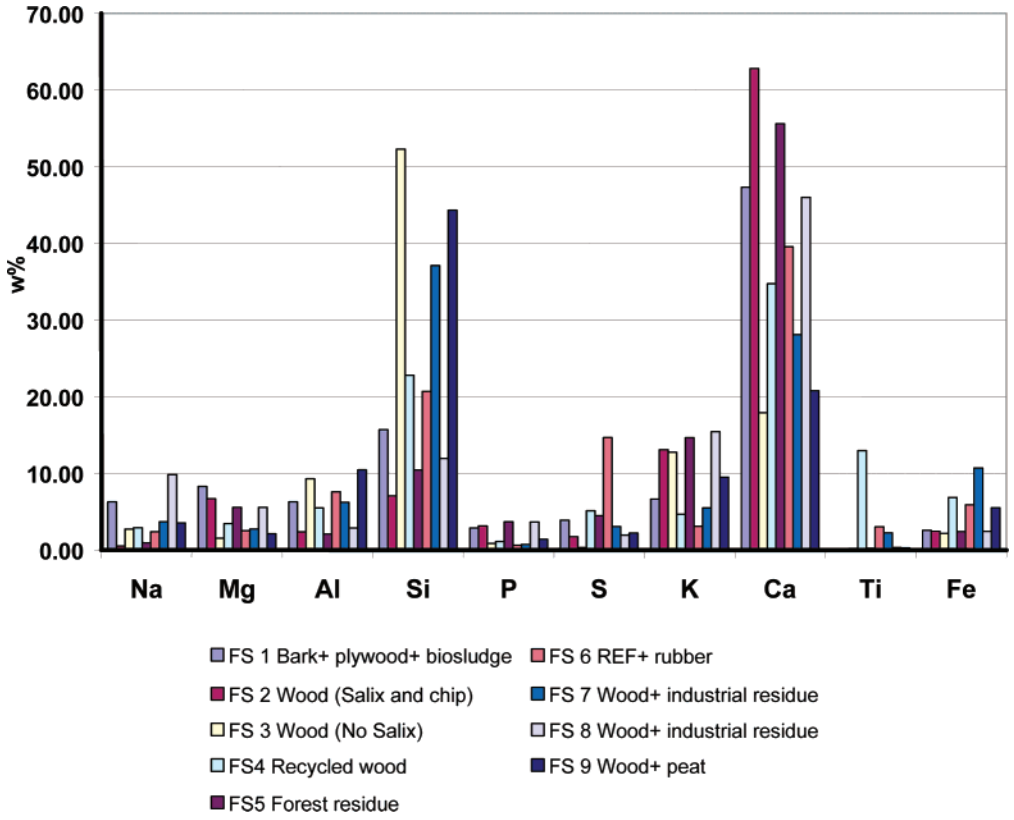

Figure 2. Bar graph showing the chemical composition of fuel ash from full-scale tests.

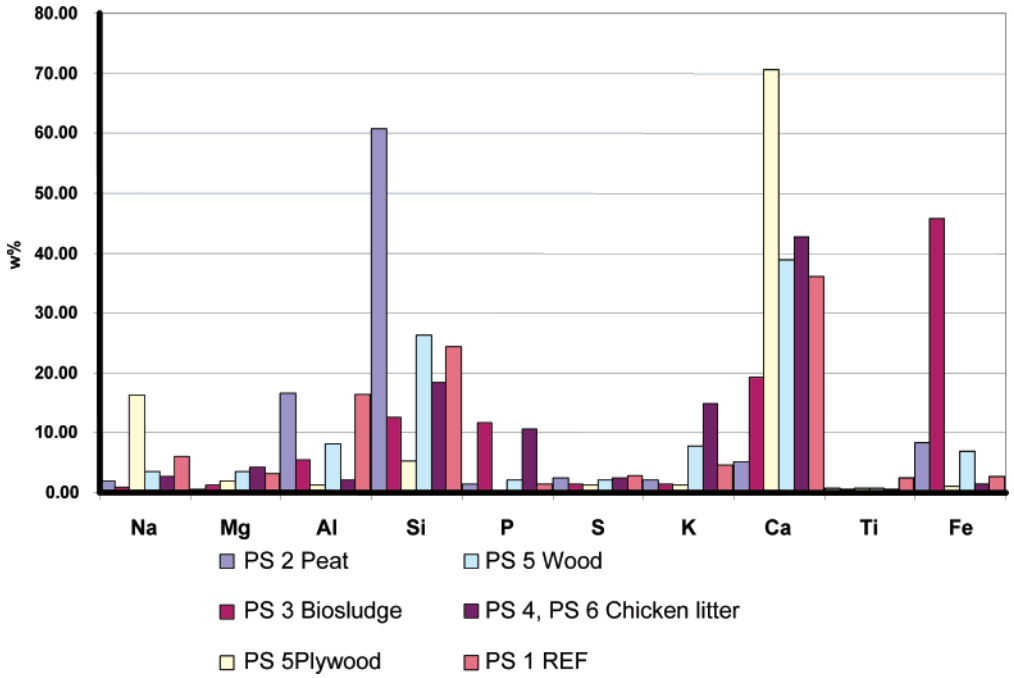

Figure 3. Bar graph showing the chemical composition of fuel ash from pilot-scale tests.

in most cases, however, that the particles are covered by coating layers of varying thickness. The effect of these coating layers on the compositional distributions, such as those shown in Figure 4, is only observed as a widening of the distribution around the maxima toward the corner defined by the sum of the calcium and iron contents. If a more detailed description of the compositional distribution of these thin coating layers is needed, it can only be provided by point analyses that are concentrated in the relevant regions.

The coating of the bed particles consisted of 1−3 superimposed layers, as exemplified in Figure 5 by a phase relationship image of a SiO_2 particle when wood is combusted in a quartz bed (test sample LS1). The combined thickness of the layers is typically 50−70 μm, with the maximum being 100 μm. The outermost layer is the thinnest (1−5 μm) and may be relatively dense. The visually dense innermost layer is 5−20 μm, and the thickness of the rather porous intermediate coating layer is 5−50 μm. Latva-Somppi et al.[17] found that the

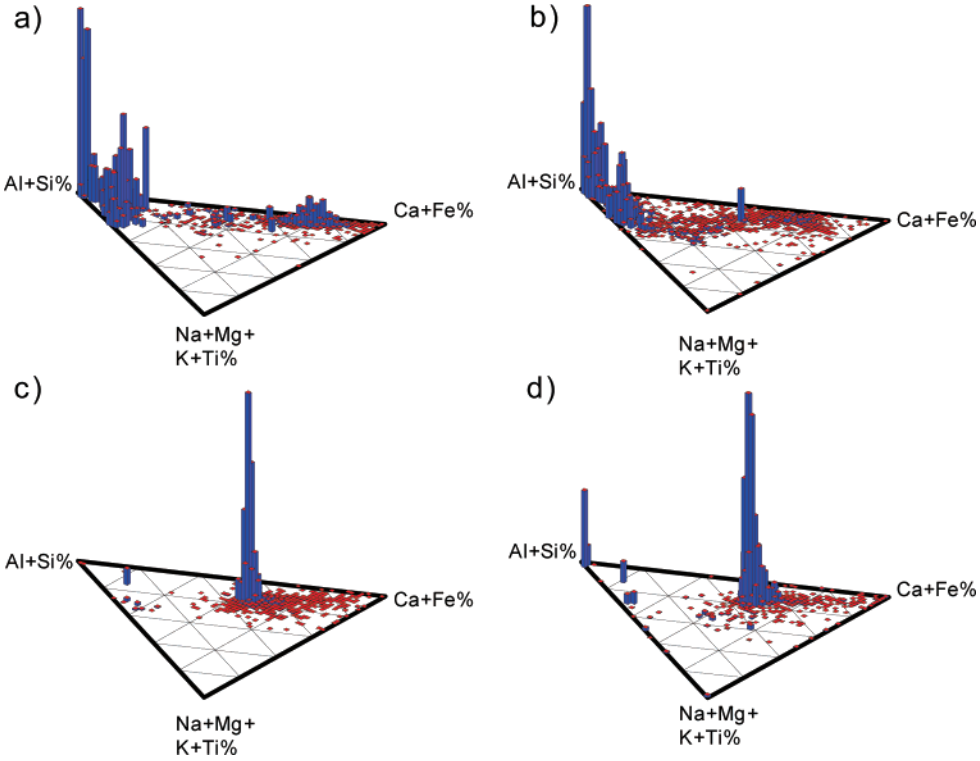

Figure 4. Quasi-ternary diagrams of bed samples from test samples (a) PS3 (fuel: biosludge), (b) FS1 (fuel: bark, plywood, and biosludge), (c) PS5 (fuel: plywood and wood), and (d) PS6 (fuel: chicken litter).

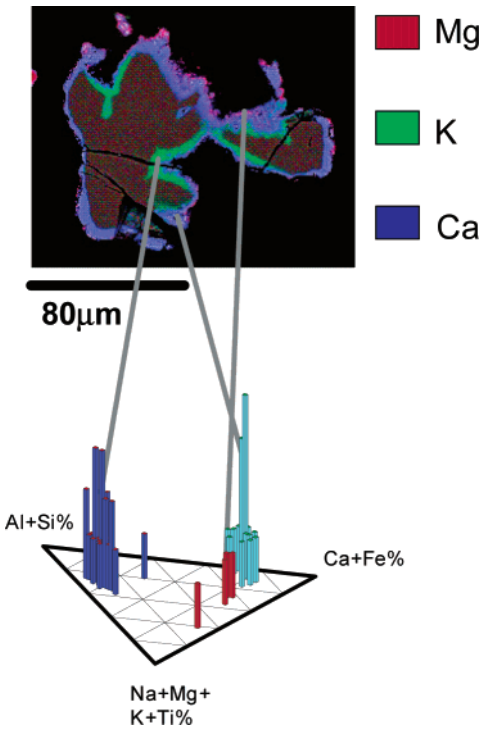

Figure 5. Point analyses of the coating layers on SiO_2 particles in the laboratory-scale test sample LS1 (fuel: wood residue); the innermost layer is shown in dark blue, the intermediate layer in light blue, and the outer in red. Analyses locations are indicated in the phase relationship image.

coating layers in the samples collected from circulating fluidized bed (CFB) units are thicker than in those collected from the bubbling fluidized bed (BFB) units. This conclusion was verified in this study. The layer growth is balanced by bed attrition, which continuously fragments the layer. The attrition is most significant for the largest bed particles, presumably because of the higher kinetic energy during fluidization.

Quartz Bed. In the vapor phase, alkali-metal compounds can react with SiO_2 and form a molten phase on the surface of the particles.[18,19] We have observed that three coating layers can typically be formed on SiO_2 particles. For the combustion of wood residue (test sample LS1) that contains potassium, the innermost coating layer contains significant amounts of potassium, as observed in Figure 5. The quasi-ternary diagram from the point analyses, as also shown in Figure 5 and the more detailed elemental composition shown in Figure 6, indicate that the innermost layer contains ca. 18%−25% potassium. This can be compared with the potassium content of ash in wood residue, which is 5.89 wt %.[8] Interestingly, the chemical composition of the innermost layer is similar to that of the adhesive material in agglomerates (see Figure 7).

The intermediate coating layer contains calcium (66%−71%) and silicon (23%−27%). The outer coating layer is enriched in magnesium (14%−37%), with the silicon and calcium contents diminished to ca. 10% and 35%, respectively (see Figure 6). Magnesium that is found in the outer layer probably originates from the fuel; its content varies considerably, even around the same particle.

(17) Latva-Somppi, J.; Kurkela, J.; Tapper, U.; Kauppinen, E. I; Jokiniemi, J. K.; Johansson, B. Ash Deposition on Bed Material Particles during Fluidized Bed Combustion of Wood-Based Fuels. In *Proceedings of the ABC '98 International Conference on Ash Behaviour Control in Energy Conversion Systems* (Yokohama, Japan, 1998); pp 110−118.

(18) Jeffers, S.; Mullen, J. F.; Cohen, A. J.; Dangtran, K. Control Problem Waste Feeds in Fluid Beds. *Chem. Eng. Prog.* **1999**, 59−63.

(19) Valmari, T.; Lind, T. M.; Kauppinen, E. I.; Sfiris, G.; Nilsson, K.; Maenhaut, W. Field Study on Ash Behavior during Circulating Fluidized-Bed Combustion of Biomass. 1. Ash Formation. *Energy Fuels* **1999**, *13*, 379−389.

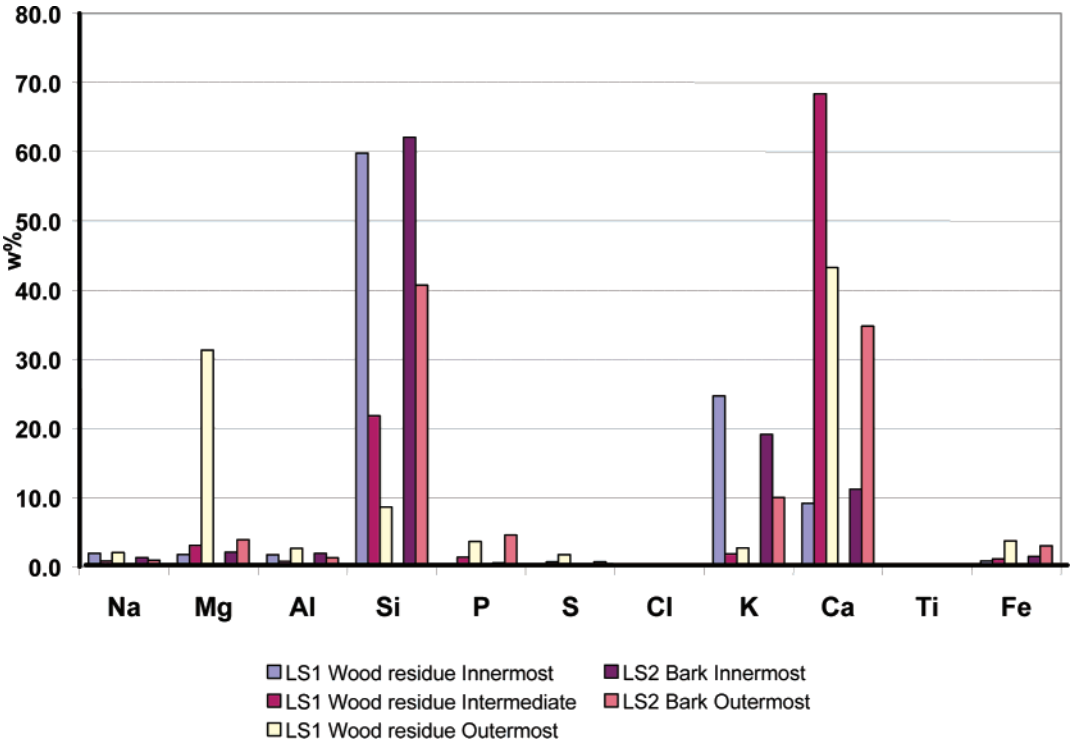

Figure 6. Diagram of the coating layers on the SiO_2 particles in the quartz bed.

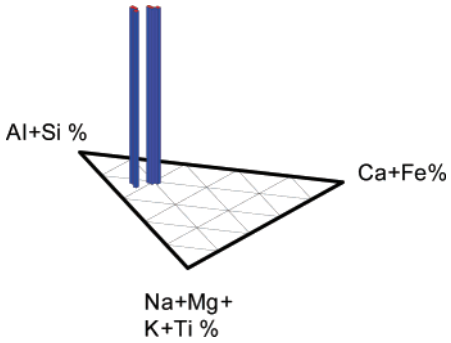

Figure 7. Average composition of the adhesive material of the agglomerates in the laboratory-scale test sample LS1 (fuel: wood residue).

The coating layers on SiO_2 particles are similar, when combusting both wood residue (test sample LS1) and bark (test sample LS2) in a quartz bed. The potassium-rich innermost layer found on the bed particles of test sample LS2 is a consequence of bark ash, which contains 6.36 wt % potassium.[8]

It can be concluded that the composition of the coating layers on SiO_2 particles follow the trend shown in Figure 8. The direction of the arrow in the figure indicates the change in the composition when moving from the inside of the particle to the surface through the coating layers. The increase of the magnesium content in the outer layer is shown as a shift toward the Na + Mg + K + Ti corner.

Latva-Somppi et al.[17] proposed that the potassium released from the fuel may react with silicon dioxide (SiO_2) in different ways:

(1) Diffusion of vapor to the surface of the bed particles, followed by a surface reaction.

(2) Deposition of submicrometer-sized K_2SO_2 particles on the bed material, followed by a reaction. Sulfur released from the reaction between K_2SO_4 and SiO_2 may be volatilized as SO_2. KOH and KCl are not present in the solid phase at the operating temperatures of the bed.

(3) Deposition of supermicrometer-sized particles on the bed material, followed by a reaction of potassium that is present in the submicrometer-sized particles with SiO_2.

The following chemical subprocesses were also suggested for bed agglomeration:[8]

(1) Ash deposition on the bed material is dominated by a combination of the attachment of small particles of submicrometer size[17] on bed particle surfaces, condensation, and chemical reaction of gaseous alkali-metal species such as KCl, KOH, or K_2SO_4 on bed particles.

(2) When the deposition on the bed particles proceeds, the inner coating layer is homogenized and strengthened via sintering.

(3) The melting behavior of the homogeneous silicate layer seems to control the adhesive forces, which are responsible for the final agglomeration process.[8]

If the alkali-metal content in the fuel is low, only one or two layers were typically observed. For instance, the potassium content of a peat ash was 1.41 wt %.[8] When this peat was combusted, only one coating layer was observed (see Figure 9). The main components in this layer are iron, silicon, and calcium. The iron content is 25%−41%, the silicon content is 23−43%, and the calcium content is 21%−26%. Öhman et al.[8] reported that this peat ash contains 17.1 wt % iron, 16.4 wt % silicon, and 14.8 wt % calcium.

Natural Sand Bed. Coatings were observed in most tests on the bed particles of the natural sand bed (test samples FS1−FS6, PS1, PS3, and PS4). As discussed previously, the natural sand bed contains several different types of particles (see Table 2), and the nature of the coating layers depends on their identity. Those on the SiO_2 particles follow the pattern discussed previously for the quartz bed. Two or three coating

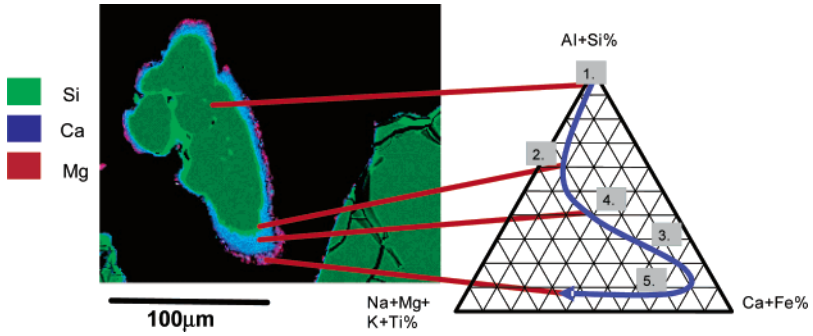

Figure 8. Phase relationship image showing the coating layers of SiO_2 particles when combusting wood residue (sample LS1). Point analyses have been performed at different locations on the coating layers and the particle: "1", the composition of pure bed particle; "2", the innermost coating layer; "4", the intermediate coating layer; and "5", the outer coating layer. The region labeled "3" indicates the composition of the innermost coating layer when the fuel does not contain significant amounts of potassium. This point has been added for comparison.

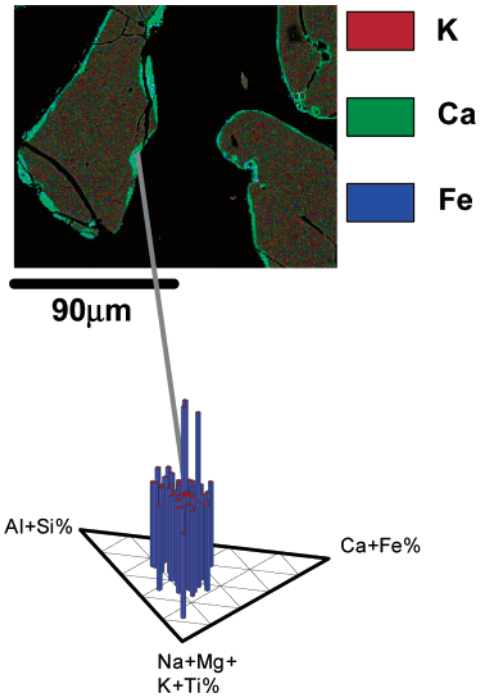

Figure 9. Point analyses of the coating layers on SiO_2 particles in the laboratory-scale test sample LS3 (fuel: peat). The innermost layer is shown in dark blue, the intermediate layer in light blue, and the outer layer in red. Analyses locations are indicated in the phase relationship images.

layers are again observed, depending on the fuel. If the alkali-metal content in the fuel was high, the innermost coating layer was alkali-rich. This can be observed in Figure 10 in the case of test samples FS3 (wood, no salix, natural sand) and FS5 (forest residue, natural sand bed). This observation is consistent with the average composition of the standard ash of the fuels in question (see Figure 2).

In general, the innermost coating layer on SiO_2 particles mainly contains silicon (20%−68%) and calcium (6%−20%). The potassium content in the innermost layer is 10%−15% and the sodium content is 1%−7%, depending on the chemical composition of the fuel ash. The content of other elements in this coating layer is <5%. The intermediate coating layer on the SiO_2 particles contains mostly calcium and silicon. As discussed previously, the magnesium content on the outer coating layer may vary significantly. It was not possible, however, to detect the magnesium-rich outer layer by SEM-EDS point analyses, because of the extreme thinness of the layer. In contrast, this layer can conveniently be observed in the X-ray maps and phase relationship images (the phase relationship image illustrating the thin coating layers is exemplified in Figure 5).

In the case of recycled wood (test sample FS4) in a natural sand bed, all layers found on the SiO_2 particles contain variable amounts of titanium (3%−30%). This could be due to additives (e.g., paints or impregnating agents) that may be present in the wood. The titanium content of the fuel ash is 13 wt % (see Figure 2). When chicken litter is combusted (test sample PS4), the content of iron increases from the inside of the particle toward the surface within every layer. The maximum iron content, 26%, was observed in the outer coating layer. The combustion of chicken litter in a natural sand bed led to fluidization problems and the testing of sample PS4 had to be interrupted within a hour. However, only a minor amount of agglomeration was observed.

The combustion of biosludge (test sample PS3) led to only one coating layer on the SiO_2 particles in the natural sand bed. This layer contained phosphorus (5%−14%), chlorine (1%−34%), and iron (27%−56%), with the remainder being silicon (16%−42%) and calcium (10%−17%). The composition of this coating layer is quite similar to the average composition of the biosludge ash (12 wt % phosphorus, 46 wt % iron, 13 wt % silicon, and 19 wt % calcium), as shown in Figure 3.

The next-abundant particles in the natural sand bed seem to be potassium aluminosilicate. Their coating layers differ from those on SiO_2 particles, because no potassium-containing innermost layer was observed. This is to be expected, because the particle itself contains potassium. It is conceivable that potassium aluminosilicate particles are not as susceptible as SiO_2 particles to potassium species in the vapor phase. The average composition of the coating layers on the potassium aluminosilicate particles, based on point analyses, is shown in Figure 11.

The magnesium content increases when moving toward the surface of the particle. At the same time, the silicon content becomes smaller. The content of other elements seem to be mostly unaffected.

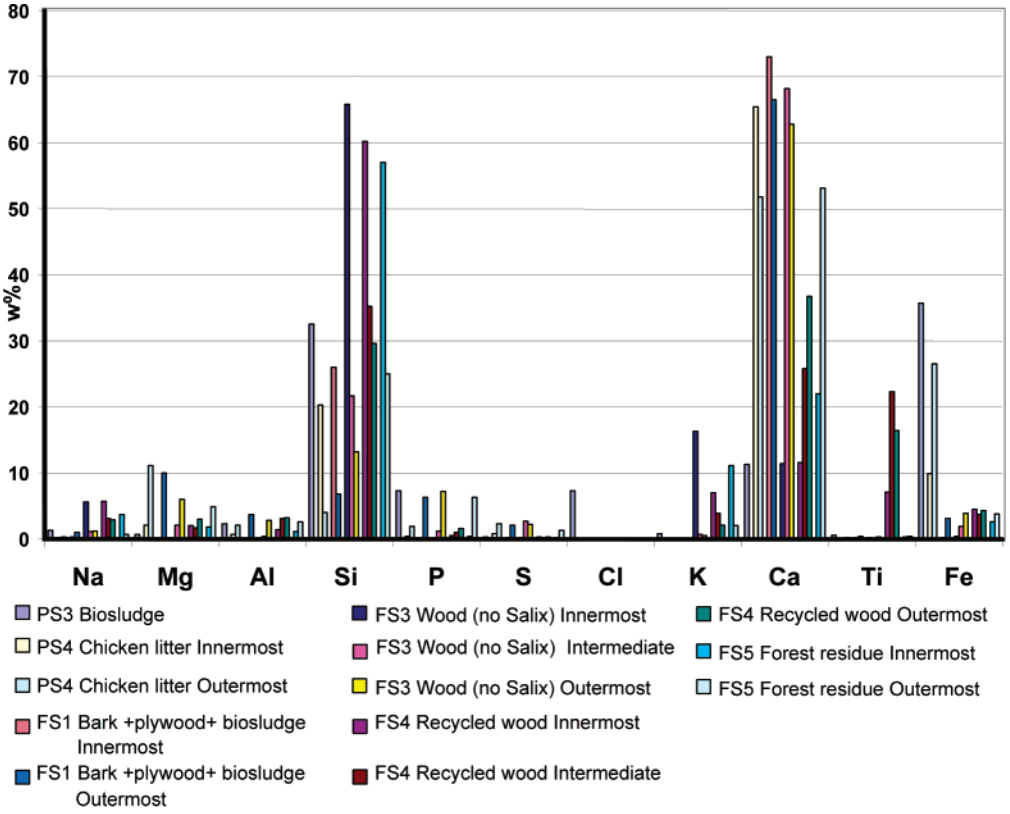

Figure 10. Bar graph showing the average composition of the coating layers on the SiO_2 particles in a natural sand bed.

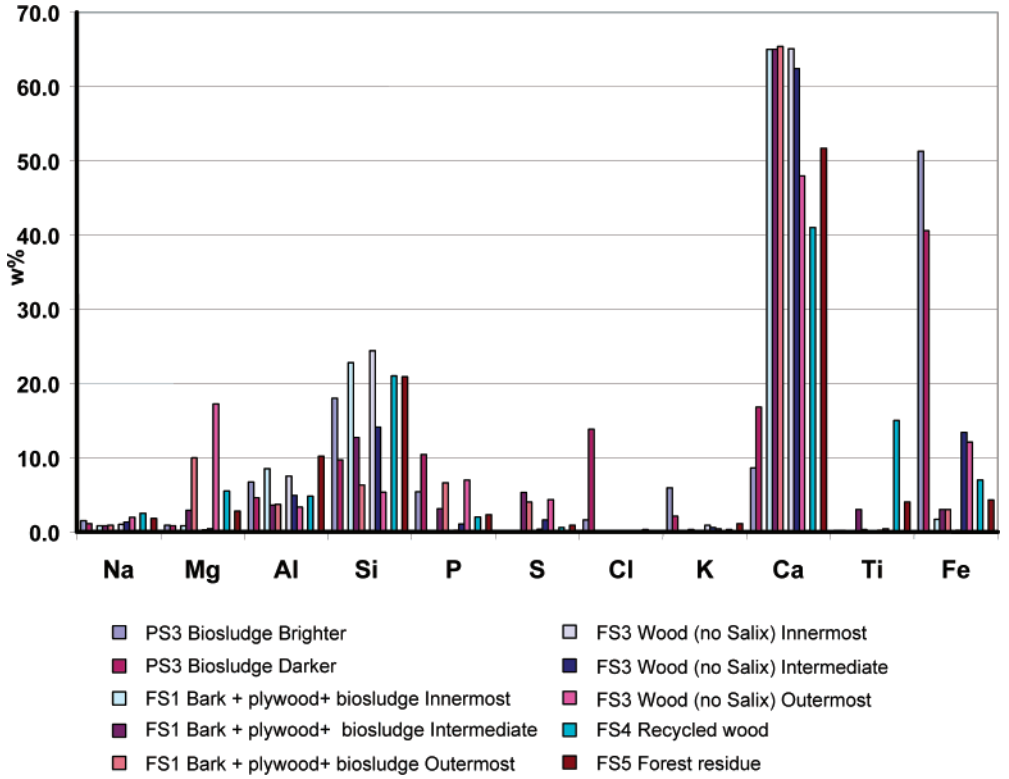

Figure 11. Bar graph showing the average composition of the coating layers on the potassium aluminosilicate particles in a natural sand bed.

The coatings on the bed particles are generally densely assembled in well-ordered superimposed layers, whereas the combustion of biosludge in a natural sand bed (test sample PS3) led to a fluffy coating on the potassium aluminosilicate particles with no well-defined layers. In contrast, these coatings exhibited discrete regions that could be divided into two main categories. Although all regions in these coatings contain relatively high iron contents, those that appear brighter in the BE image contain more iron than those that appear darker. In contrast, the darker regions contain much more chlorine. In addition, the brighter regions contain

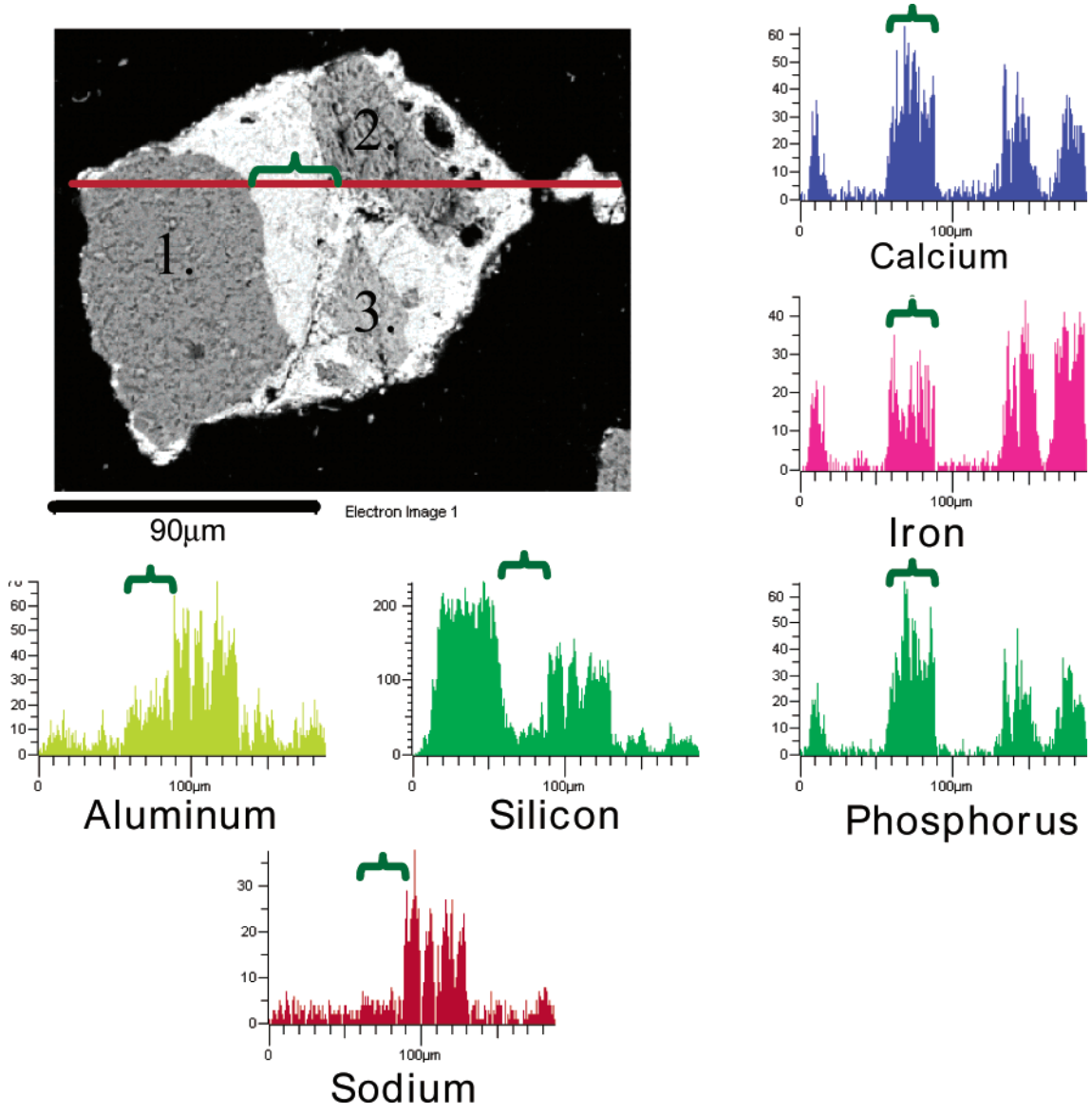

Figure 12. Line scan of the agglomerate found in test sample PS3: region 1 is a silicon dioxide particle; region 2 is a sodium aluminosilicate particle; and region 3 is a potassium aluminosilicate particle.

less phosphorus and calcium, and more silicon, than the darker regions.

Agglomerates were generally found in tests that involved a natural sand bed. In most cases, the adhesive material was potassium-rich and resembled the innermost coating layer. In test sample PS3 (biosludge, natural sand), however, the composition of the adhesive material in agglomerates was 16% silicon, 17% phosphorus, 20% calcium, and 40% iron, with no significant amounts of potassium. The analytical results are reported as average values from several point analyses from different portions of the adhesive material.

The trends in the composition of the agglomerate formed during the testing of sample PS3 (biosludge, natural sand) is shown by the line scan shown in Figure 12. Interestingly, the adhesive material binds together three types of particles: silicon dioxide (SiO_2), potassium aluminosilicate, and sodium aluminosilicate. The line scan across the agglomerate is indicated in Figure 12. Particle 1 in the figure is virtually pure SiO_2. The silicon content decreases at the surface of the particle, and the adhesive material is, indeed, rich in iron, calcium, and phosphorus. The high iron content probably has a significant role in the formation of the agglomerate in this case.

Although the compositions of the coatings on the sodium aluminosilicate particles and sodium calcium aluminosilicate particles that were also found in the natural sand bed generally reproduced the trends previously discussed for the coatings on the potassium aluminosilicate particles, there were cases (e.g., test samples FS3 (wood, no salix, natural sand) and PS4 (chicken litter, natural sand)) where the potassium-rich innermost layer could be detected. Interestingly, in test sample FS5 (forest residue combusted in a natural sand bed), potassium was found enriched in the outermost layer, but not in the innermost layer.

In test sample PS3 (biosludge, natural sand), only one coating layer was observed on the sodium calcium aluminosilicate particles. As discussed previously, the SiO_2 particles of this natural sand bed also exhibited only one coating layer during the combustion of biosludge. The main difference in the compositions of the coating layers on these two particles involved the lack

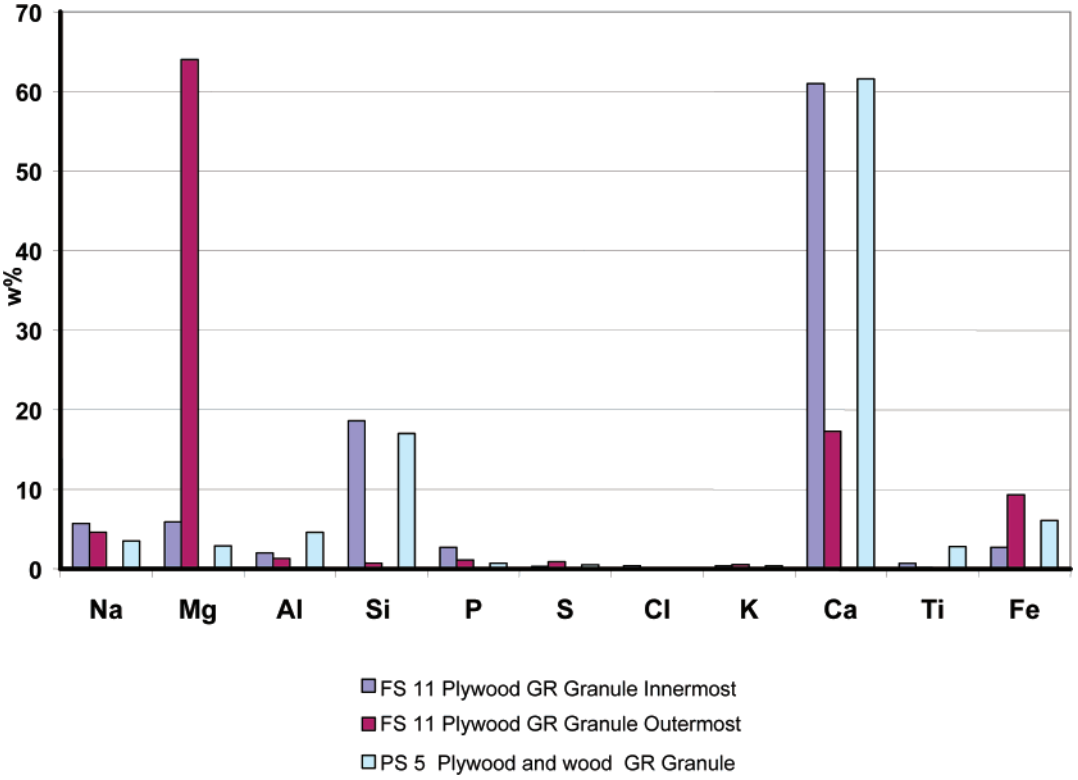

Figure 13. Bar graph showing the average composition of the coating layers on the GR Granule particles.

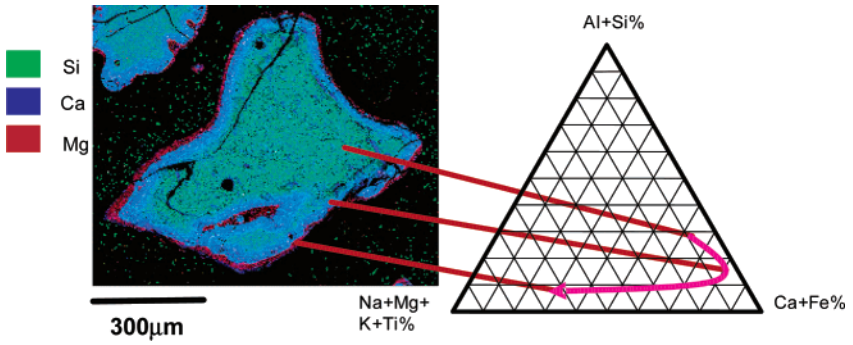

Figure 14. Phase relationship image and the compositional trends in the coating layers of the GR Granule particles.

of chlorine on the coating of the sodium calcium aluminosilicate particle. The coating layers on sodium aluminosilicate particles in test sample PS3 (biosludge, natural sand) were too thin to be analyzed quantitatively and were only detected in X-ray maps.

GR Granule Bed. The SiO_2-free GR Granule bed has been found to be suitable for the combustion of fuel with a high alkali-metal content. Although a coating was observed on all bed particles in all tests, with the sole exception of test sample PS6 (chicken litter, GR Granule bed), which showed no coating layers, virtually no agglomeration was observed. The average composition of the coating layers of the GR Granule particles, based on point analyses, is shown in Figure 13. The GR Granule particles in test samples FS10−FS13 were coated with two superimposed layers, as illustrated by the phase relationship image in Figure 14. The figure shows that the innermost layer is calcium-rich and the thin outermost layer is magnesium-rich. The combination of the point analyses with the phase relationship image indicates that the magnesium content increases up to 70% when moving from inside the particles to the outer coating layer (see the quasi-ternary diagram in Figure 14). The innermost layer contains 40%−65% calcium and 15%−20% silicon. It is the magnesium-rich outer layer that is thought to protect the particles against agglomeration. This conclusion can be supported by the observation that the same type of coating layers have been found on the particles of the natural sand bed when dolomite has been added to prevent agglomeration.[20] Furthermore, no magnesium-rich regions have been observed in the agglomerated beds. In the GR Granule bed, the magnesium originates from the attrition of the bed particles. The magnesium-bearing compounds have been found to be effective in controlling ash-related problems, whereas high levels of calcium have been found to delay and decrease the severity of agglomeration.[21] The outer layer is very rich in mag-

(20) Daavitsainen, J.; Nuutinen, L.; Ollila, H.; Tiainen, M.; Laitinen, R. FB Combustion of Bark and Sawdust in Silica Sand Bed with Dolomite Addition. A Case Study. In *16th International Conference on Fluidized Bed Combustion* (Reno, NV); Geiling, D. W., Ed.; American Society of Mechanical Engineers (ASME): New York, 2001.

(21) Vuthaluru, H. B.; Zhang, D.-k. Effect of Ca- and Mg-Bearing Minerals on Particle Agglomeration Defluidisation during Fluidised-Bed Combustion of a South Australian Lignite. *Fuel Process. Technol.* **2001**, *69*, 13−27.

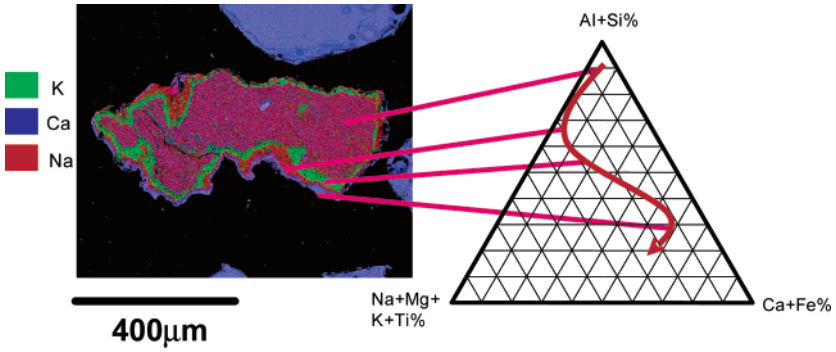

Figure 15. Phase relationship image and the compositional trends in the coating layers of the sodium aluminosilicate particles in a GR Granule bed.

nesium; therefore, it is conceivable for this sample to have a high melting point. We note that pure magnesium oxide melts at 2825 °C.[21]

Some tests showed exceptional behavior. The combustion of chicken litter (test sample PS6) also led to a fluidization problem with a GR Granule bed in a similar fashion as that in the case of a natural sand bed. As observed in test sample PS4 (chicken litter, natural sand), the fluidization problems in sample PS6 were not caused by agglomerates and the bed particles showed no coating layers. In test sample FS8, where wood and industrial residue were combusted in a GR Granule bed, two layers could be observed; however, neither layer contained magnesium. The innermost coating layer was calcium-rich (43%−56%) and also contained 17%−36% silicon and 2%−17% iron. In the outer coating layer, the silicon content was 19%−68%, the calcium content was 10%−47%, and the sodium content was 3%−30%.

The GR Granule bed contained small amounts of magnesium iron silicate particles, the innermost coating layer of which was rich in calcium (53%−67%) and silicon (15%−21%). The outer layer was mainly magnesium-rich material (33%−66%) that also contained 8%−40% calcium and 2%−10% silicon. The chemical composition of the calcium-containing layer was very similar to the calcium-containing layer on the GR Granule particles; however, the magnesium content in the outer layer of the magnesium iron silicate particle was less than that in the corresponding layer on the GR Granule particle. Sodium was determined to be evenly distributed in both coating layers of the magnesium iron silicate particles, but the phosphorus content increased toward the outer layer.

The GR Granule bed also contains sodium aluminosilicate and sodium calcium aluminosilicate impurities. Interestingly, although the sodium aluminosilicate and sodium calcium aluminosilicate in the natural sand bed did not indicate potassium-rich innermost layers, they were present on these particles in every test that involved a GR Granule bed. When the fuel contained alkali-metal species, the composition of the innermost layer consisted of 25%−30% of these elements. This is clearly seen in Figure 15, where a mixture of plywood and wood was combusted (test sample PS5, GR Granule). The innermost coating layer contained potassium, and the intermediate coating layer contained sodium (see Figure 15). The source of sodium in the fuel originates from the plywood (see Figure 9). We note that the sodium aluminosilicate and sodium calcium aluminosilicate particles both show a potassium-rich innermost layer, in a fashion similar to the SiO_2 particles in the natural sand bed. This innermost coating layer contained 26%−32% potassium. Because GR Granule bed particles are SiO_2-free and do not react with the vapor of alkali-metal species, it is probable that potassium is enriched in the innermost layer as a consequence of the interaction of the potassium compounds with the sodium aluminosilicate and sodium calcium aluminosilicate particles. The intermediate and outermost layers on the sodium aluminosilicate and sodium calcium aluminosilicate particles resemble those of SiO_2 particles.

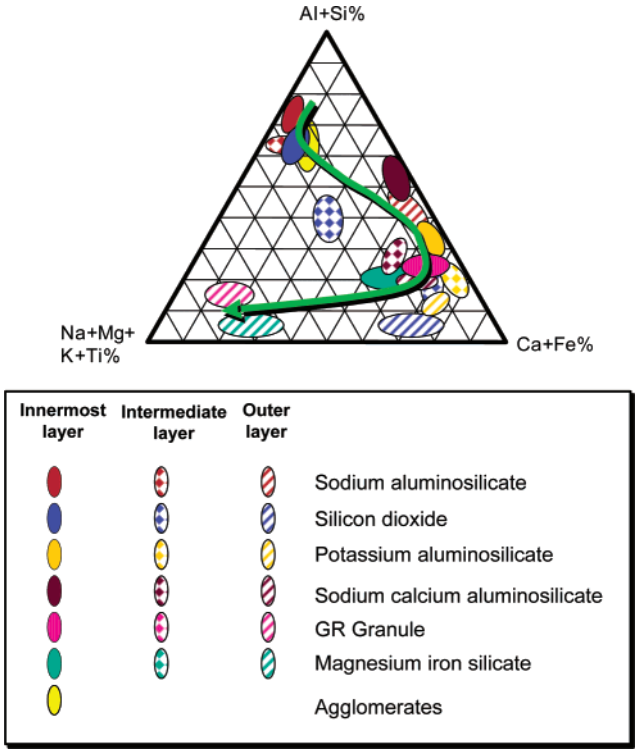

Figure 16. Compositional trends in the coating layers when combusting biomass fuels in a fluidized-bed boiler utilizing different bed materials.

Conclusions

The formation of coating layers on particles of different bed materials (quartz, natural sand, and GR Granule) has been studied in the fluidized-bed combustion of various biomass fuels (bark, different types of wood fuel, peat, biosludge, chicken litter, REF, and forest residue). The chemical composition of the coating layers

were characterized by scanning electron microscopy, coupled with energy-dispersive spectroscopy (SEM-EDS), through the utilization of line scans, as well as point and domain analyses. X-ray maps were also recorded to characterize the coating layers.

With the exception of quartz, which showed the presence of 100% silicon dioxide (SiO_2) particles, the bed materials were heterogeneous mixtures. Natural sand contained SiO_2 particles, potassium aluminosilicate particles, sodium aluminosilicate particles, and sodium calcium aluminosilicate particles. The GR Granule material also showed the presence of potassium aluminosilicate, magnesium iron silicate, sodium aluminosilicate, sodium calcium aluminosilicate, and SiO_2 particles as minor components.

The compositions of the coating layers on the bed particles were dependent both on the nature of the bed particles and the fuel used in the combustion and showed some general features. There were generally 1−3 superimposed coating layers on the different bed particles, and their composition exhibited similar trends in every case, as shown in Figure 16. The composition of the layers varied according to the arrow in the figure when moving from the innermost layer toward the surface of the particles. Interestingly, the composition of the innermost layers on both SiO_2 and sodium aluminosilicate particles resembles that of the adhesive material of the agglomerates. Therefore, it is conceivable that the coating layers that contain potassium or sodium may be adhesive and cause the formation of agglomerates. The outer coating layers in the bed particles that involve GR Granule are magnesium-rich. This layer is thought to protect the bed from agglomeration. In fact, generally no problems were encountered when even problematic fuels, such as plywood, were combusted in a GR Granule bed.

Acknowledgment. Financial support from Technology Development Centre Finland and Academy of Finland is gratefully acknowledged. The samples in this study were supplied by Energy Technological Centre (Piteå), Foster Wheeler, Fortum, and Putkimaa.

EF0300850